Article

Not peer-reviewed version

Optical Properties, Thermal Stability, and Biological Activity of a Non-Centrosymmetric Hybrid Compound 3,4-Diaminopyridinium Perchlorate (3,4-DAPP)

Soulayma Mtar , Sameh Sellami , Nassira Chniba-Boudjada , Mohamed Boujelbene *

Posted Date: 9 October 2024

doi: 10.20944/preprints202410.0601.v1

Keywords: non-centrosymmetric hybrid; supramolecular; crystal voids; optical property; DFT calculation; in-vitro antibacterial

Article

Optical Properties, Thermal Stability, and Biological Activity of a Non-Centrosymmetric Hybrid Compound 3,4-Diaminopyridinium Perchlorate (3,4-DAPP)

Soulayma Mtar [1], Sameh Sellemi [2], Nassira Chniba-Boudjada [3] and Mohamed Boujelbene [1,*]

[1] Laboratory of SolidState Physics and Chemistry,LR11 ES51, department of chemistry, Facultyof Sciences of Sfax, Universityof Sfax, 3071 Sfax, Tunisia.
[2] Biopesticides Laboratory, Centre of Biotechnology of Sfax, Sfax University, P.O. Box '1177' 3018, Sfax, Tunisia
[3] Laboratory of Crystallography, CNRS, 25 Martyrs Avenue, 166, 380 Grenoble, France
* Correspondence: m_boujelbene2010@yahoo.fr

Abstract: In this work, a new hybrid compound3,4-diaminopyridinium perchlorate with the formula ($C_5H_8N_3$)ClO_4abbreviated 3,4-DAPP was synthesized in aqueous solution at room temperature by the slow evaporation method. It crystallizes in the monoclinic system,with a non-centrosymmetric space group $P2_1$with the following parameters: a=5.1261 (9), b=9.3003 (17),c=8.6659 (16) Å and β=102.595 (7) °. However, the supramolecular crystal structure was built from perchlorate anions $(ClO_4)^-$ and organic diaminopyridinum cations $(C_5H_8N_3)^+$connected with hydrogen bonds to form a three-dimensional network. Fourier transform infrared (FTIR) and Raman spectra indicate that the vibrational modes correspond to both inorganic and organic entities. According to Hirschfeld's analysis, the crystal packing is mainly stabilizedby the presence of hydrogen bonds O···H (50%), as well as the crystal void analysis indicates the mechanical stability of the structure. Furthermore, the thermal behavior studied by thermogravimetric (TGA-DTA) and differential scanning calorimetry (DSC) appears to have good stability up to 280°C. Finally, the optical properties were investigated by UV-Vis absorption and photoluminescence spectroscopy along with density-functional theory DFT calculations, whichexhibit emission property, and a band gap energy of 3.9 eV.Additionally, biological activity tests revealed that 3,4-DAPP exhibited moderate antibacterial activity, particularly against Bacillus cereus, though it was less effective than 3,4-diaminopyridine (3,4-DAP) against several other bacteria, indicating that the perchlorate group in 3,4-DAPP may reduce its antimicrobial efficacy.

Keywords: non-centrosymmetric hybrid; supramolecular; crystal voids; optical property; DFT calculation; in-vitro antibacterial

1. Introduction

Current research on organic-inorganic hybrid materials has gained much importance in recent years due to the manufacturability and diversity of physicochemical properties of various materials, which could be used in a wide range of applications, such as optics[1,2], photovoltaic [3], catalysis [4] and other fields [5,6]. This research has mainly focused on the optical properties of hybrid materials due to their strong room-temperature emission. Moreover, by substituting halogen or metal sites through theappropriate choice of organic components, it is conceivable to govern the particular structure of the inorganic-organic sheets, which makes it possible to control the physical properties of these compounds. In almost all of the considered materials, aminopyridines are bioactive N-heterocyclic tertiary amines, particularly relevant since they significantly increase the amount of acetylcholine produced in response to conduct nerve impulses as well as electronic depolarizations of tetrodotoxin-blocked motor nerve terminals [7]. In addition, these heterocyclics show great promise as potassium channel blockers, especially giventheir high potency, high specificity of

 doi:10.20944/preprints202410.0601.v1

potassium channels (K^+), and effectiveness in pharmacological dissection of the ionic channels of excitable membranes [8]. Due to their ability to improve nerve transition, aminopyridines have been offered as treatments for multiple diseases such as sclerosis [9], myasthenia gravis [10], Alzheimer's[11], anesthesia, and muscle relaxation [12]. This feature makes it widely used and has been created using compounds derived from heterocyclic molecules, amongst one of these derivates we chose to work with 3,4-diamonopyridines and perchloric acid. As a part of our ongoing work on similar structures [13–15], we report the chemical preparation, the structural study, the spectroscopic measurement, the thermal behavior,and finally the biological test of the title compound.

2. Materials and methods:

2.1. Synthesis

The crystals of 3,4- diaminopyridinium perchlorate with the formula $(C_5H_8N_3)ClO_4$ were obtained due to a solution of concentrated $HClO_4$acid (Sigma Aldrich 92%) and the organic molecule 3,4-DAP (3,4-diaminopyridine) (Sigma Aldrich 98%) in stoichiometric ratio 1/1. The reaction was carried out in the presence of water (10ml) and maintained at room temperature. The reaction sequence for the synthesis is reported in the following equation:

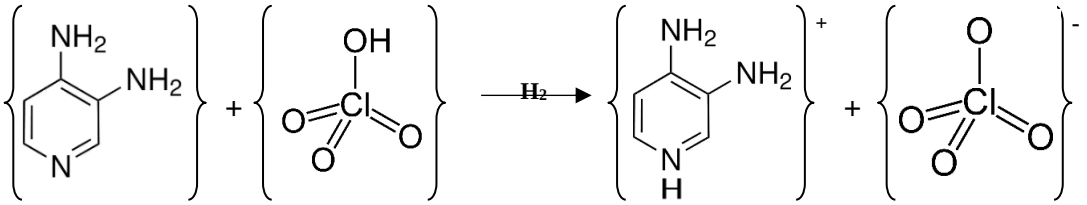

After several days of evaporation, transparent prism crystals appeared in the solution then isolated and dried in the air.

2.2. Spectroscopic Measurements

The sample's infrared spectrum was recorded at ambient temperature using a Perkin-Elmer FT-IR 100 spectrometer in the region 4000-400 cm^{-1}. The RAMAN spectrum was recorded using a Horiba JobinYvon triple monochromator spectrophotometer (Lab RAM HR 800) in the range of 50 to 4000 cm^{-1}. Both spectra were recorded at the same resolution (50 cm^{-1}) with 3 $cm^{-1}$of spectral steps.

2.3. X-ray Data Collection and Structure Determination

In order to define the crystal structure, a suitable crystal of $(C_5H_8N_3)ClO_4$ was selected and characterized on a diffractometerBrukerApexII, Kappa CCD type, equipped with graphite-monochromated Mo K_α radiation ($\lambda = 0.71073$ Å), and it was maintained at 200 K during data collection. The crystal structure was solved using the WingX software [16],using the SHELXT 2018.2 [17] structure solution program and refined with the SHELXL-2018.3 refinement package.The positions of all H-atoms were fixed geometrically by the appropriate instructions HFIX.The crystallographic data as well as some details of the structure refinement results are provided in Table 1.

Table 1. Crystal data and structure refinementdetails of 3,4- DAPP.

Crystallographic data	
Chemical formula	$C_5H_8N_3ClO_4$
Color/form	Colorless / Prism
Formula weight (g/mol)	209.59
Cell volume Å³	403.2 (12)
Density (Mg m⁻³)	1.726

 doi:10.20944/preprints202410.0601.v1

Crystal system	Monoclinic
Space group	$P2_1$
Z	2
Cell parameter	
a (Å)	5.1261 (9)
b (Å)	9.3003 (17)
c (Å)	8.6659 (16)
β (°)	102.595 (7)
Radiation of Mo	Monochromatique Kα
Diffractometer	APEX II, KAPPA CCD
Intensity collection condition	
Temperature (K)	293 K
Wavelength (Å)	0.71073
Indexe range	-6<h<6 ; -10<k<10 ; -10<l<10
Total number of recorded reflections	19905
Total number of independent reflections	1361
Domain of θ(°)	2.4 < θ <24.7
Structure determination and refinement	
reflexions with I>2σ (I)	1327
F(000)	216
Refined parameters	121
Flack parameter	0.48
Electronic density (e Å-3)	-0.43<Δρ< 0.33
wR (F2)	0.113
R [F2> 2σ(F2)]	0.041
S = GooF	1.09
CCDC	2300737

2.4. Hirschfeld Surface Calculations

Hirschfeld surface analysis serves as an effective tool for studying the solid-state behavior of molecules as well as defining the various intermolecular interaction types in the studied compound. Molecular Hirschfeld surfaces are constructed using the distribution of electrons calculated as the sum of spherical atom electron densities [18,19]. The identification of contacts is made possible via the normalized contact distance (d_{norm}) relating to the distances from the surface to the nearest core inside and outside the surface (d_i and d_e, respectively) and the van der Waals radii (vdw) of the atom given by the equation below:

$$d_{norm} = \frac{d_i - r_i^{vdw}}{r_i^{vdw}} + \frac{d_e - r_e^{vdw}}{r_e^{vdw}}$$

where r_i^{vdw} and r_e^{vdw} are the Van der Waals radiations of the corresponding inner and outer surface atoms, respectively. Hirschfeld surface was mapped using a red, blue, and white color scheme. The red region indicates the proximity of the hydrogen bond donors to the acceptors and a negative d_{norm} value. The blue region indicates the distance of the hydrogen bond from the donor to the acceptor and a positive d_{norm} value. The white region indicates the contact distance, which is equal to zero, and indicates the normalized contact distance of hydrogen bond donors to acceptors.

2.5. Thermal Analysis

Thermogravimetric analysis (TGA) was carried out using a multi-module 92 SETA RAM analyzer from room temperature up to 500 °C, with a heating rate of 10°C/min under Oxygen gas. Also, theDifferential Scanning Calorimetric (DSC) of the title compound was performed on crystals (m = 4.4 mg)using a Perkin-Elmer analyzer, in a temperature range of -50 to 300°Cwith a heating rate of the order of 5°C/min under constant N_2 flow.

 doi:10.20944/preprints202410.0601.v1

2.6. Optical Study

The absorption spectrum of UV/vis was captured at room temperature using a HELIOS OMEGA v8. 01 spectrometer with a wavelength range of 200-600 nm and H_2O was used as a reference. Using a Perkin Elmer LS-55 spectrometer, the photoluminescence spectrum was recorded over the 200-800 nm range and exited with 340 nm radiation.

2.7. Computational Details:

All calculations were performed by using the Gaussian 09 program [20]. The density functional theory at the B3LYP level optimized the ground-state geometric structure, employinga 6–31G+ (d) basis set. Frequency calculationswere performed to confirm that the geometry is at a global minimum and has no imaginary frequencies.The electronic transitions were calculated using Density Functional Theory(DFT) at the same level. The theoretical absorption spectrum simulation (GAUSSIAN spread model at an HWHM of 20 nm) and the isodensity molecular orbitals generation were performed using the GABEDIT 2.1.0 software [21].

2.8. Determination of In-Vitro Antibacterial Activity by Agar Well Diffusion Method

Six pathogenic bacteria including 3 gram-positive bacteria, *Staphylococcus aureus*, *Bacillus cereus* and *Bacillus subtilis* and 3 gram-negative bacteria, namely *Pseudomonas aeruginosa*, *Enterococcus faecalis,*and *Salmonella typhimurium* were used in this assay.

A volume of 100 µl suspension, having 10^6 CFU/ml of each bacterial strain, was dispensed on a nutrient agar medium. Wells of approximately 10 mm was bored using a well cutter. A volume of 100 µl of 3,4-DAPP samplefrom the concentrations of 50 and 100 mg/ml were added to the wells. The plates were then incubated at 37 °C for 24 h. The antibacterial activity was assayed by measuring the diameter of the inhibition zone formed around the well. The 3,4-DAP was used as a negative control and the gentamycin antibiotic was used as a positive control [22].

3. Result and Discussion

3.1. Crystal Structures

The 3,4-diaminopyridinium perchlorate $(C_5H_8N_3)ClO_4$ is built up of ClO_4^- tetrahedra and 3,4-diaminopyridine (3,4-DAP) cations.This compound crystallized in a monoclinic system, with a non-symmetric space group $P2_1$, two units per cell (Z=2) and the following lattice parameters: a= 5.1261 (9), b= 9.3003 (17), c=8.6659 (16) Å, β=102.595 (7)° and V= 403.2 (12) $Å^3$ (Table 1). Figure 1 depicts the asymmetric unit, showcasing a protonated cation-anion par linked by a hydrogen bond.

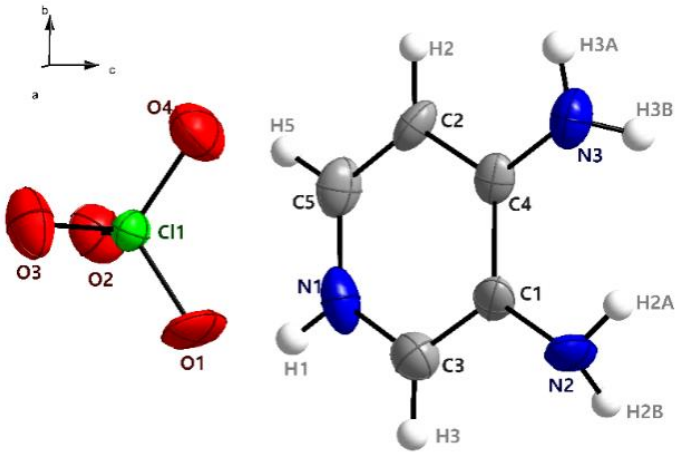

Figure 1. Asymmetric unit of$(C_5H_8N_3)ClO_4$.

Preprints.org (www.preprints.org) | NOT PEER-REVIEWED | Posted: 9 October 2024 doi:10.20944/preprints202410.0601.v1

The crystal structure displays significant inversion symmetry breaking, as supported by a Flack parameter of 0.48, indicating an asymmetric arrangement of chiral molecules. Furthermore, the cumulative intensity distribution curve suggests that the crystal data are more likely acentric than twinned or centric, providing additional evidence. The arrangement of the crystal structure is organized with parallel inorganic segments interspersed by organic chains aligning along the $\vec{b}$-axis, as illustrated in Figure S1.

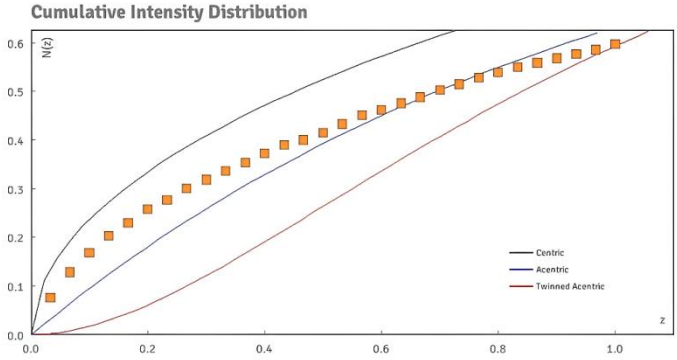

Figure 2. Cumulative intensity distribution curve of the structure data of 3,4-DAPP.

An examination of the organic component reveals 3.4-DAP cations trapped in the spacing between perchlorate tetrahedra (Figure 3a) along the [010] orientation, linked by N-H···O bonds ranging from 2.3533 to 2.5161 Å. Furthermore, the distance between aromatic nuclei measures 5.12 Å, surpassing the typical π-stacking distance (>3.8 Å), thus indicating the absence of π- π interaction within the structure [23].Conversely, the inorganic component exhibits four-coordination with $(C_5H_8N_3)^+$ cations across a similar distance spectrum as the organic part. This form of weak hydrogen bonding creates a supramolecular crystal characterized by an infinite zero-dimension network, comprising four distinct types of networks labeled $R_4^4(19)$, $R_2^1(7)$, $R_4^2(8)$ and $R_4^3(17)$ in according with Bernstein's theory nomenclature [24] (Figure 3b). Analysis of the geometric attribution of the perchlorate tetrahedra and the computed average Baur distortion indices {ID (Cl-O)= 0.003, ID (O-Cl-O)= 0.0046, and ID (O-O)= 0.0088} (Table S1), indicates a slightly distorted tetrahedral configuration, albeit describable as regular, which correlates with the stereochemical behavior of ClO_4^- anions and their hydrogen bond interactions [25]. Detailed hydrogen bond geometries are provided in Table S2.

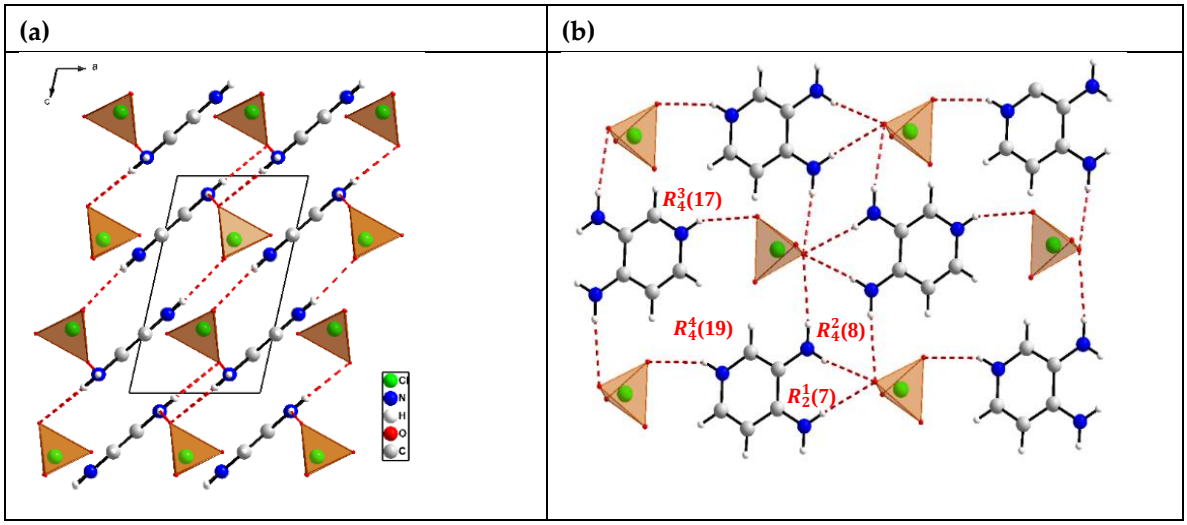

Figure 3. Structure arrangement (a), the coordination of the organic - inorganic parts, and the various circular rings (b) presented in 3,4-DAPP.

 doi:10.20944/preprints202410.0601.v1

3.2. Vibrational Spectroscopy Measurement:

For more information about the crystal structure results, we recorded the infrared (IR) and RAMAN spectra of 3,4-DAPP at room temperature.The experimental IR, RAMAN and computed IR vibrational frequencies are listed in Table S3. The most typical features in this regard are the characteristics bands of the 3,4-diaminopyridine skeleton vibrations between 3082 and 3319 cm^{-1}in the IR spectra (Figure 4), which is assigned to the symmetric and asymmetric stretching modes of NH_2 group, and out of plane deformation of the same group observedat 615 and 1635 cm^{-1}[15].For the NH^+ stretching and deformation vibration, they presented with the associated range of bands between 2029 - 2575 cm^{-1}and1355 - 1507 cm^{-1}, respectively. The out-of-plan deformation of the (C-C-C) and (C-N) of the aromatic ring appears between 544 - 554 cm^{-1} and 594 - 607 cm^{-1}, respectively.Concerning the vibrational modes of the inorganic part (ClO_4^-), the tetrahedral geometry admits four deformation modes, two in plan deformation (stretching) represented by ν_1 (ClO_4^-) and ν_3 (ClO_4^-)observed in regions between 926 and 1060 cm^{-1} in the IR spectra, and two out of plan deformation (wagging) represented by ν_2 (ClO_4^-) and ν_4 (ClO_4^-) observed at lower regions between 451 and 622 cm^{-1} in the RAMAN spectra.[23].The strong luminescence of the studied compound is confirmed by the unique curve displayed in the RAMAN spectra (Figure S2). The experimental and computed FT-IR frequencies are both consistence (Figure 4).

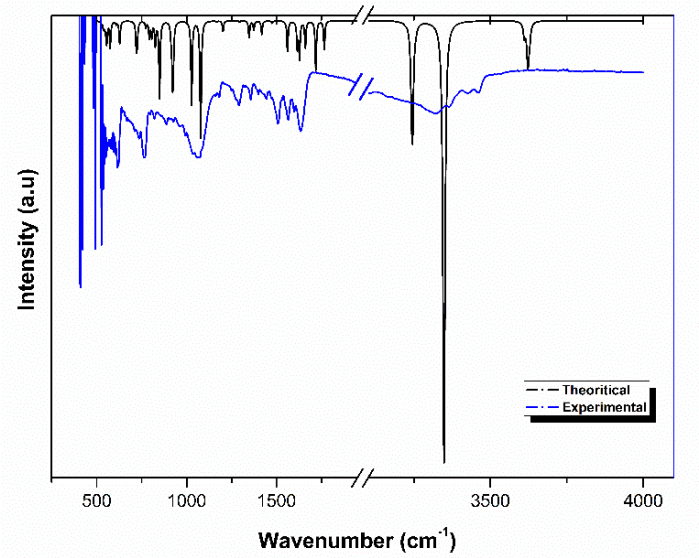

Figure 4. Experimental and theoretical IR spectra of 3,4-DAPP.

3.3. Hirschfeld Surfaces and Crystal Voids

The use of Hirschfeld surface analysis is to measure and display the close connections between atoms in the crystal structure of 3,4-DAPP. The way molecules in a crystal interact with each other is shown on HS plotted over d_{norm} (Figure S3b), where the intensive bright red spots on the surface related to the O···H/H···O interactions, while the blue regions correspond to longer contacts with positive d_{norm}value [26].The pie chart (Figure S3a) summarizes the considerable contributions from several intermolecular interactions on the Hirschfeld surface (HS). The integration of thecrystal packing is mainly assured by N-O···H interactions,which constitute half of the total interactions (50%). The H···H contacts are distributed as widely scattered points of the high density of (d_i, d_e) pairs with 19%. However, some minor intermolecularinteractions such as C···H, N···H, C···,O and others, exhibit relative contribution interactions extended between 6 and 9%.Moreover, the shape index is highly sensitive to very subtle changes in surface shape. Indeed, the relative placement of red and blue adjacent strangles on a shape index map provides insight into the interaction between π electrons. Notably, these strangles are absent from the picture (Figure S4a.), indicating the lack of π–π stacking in this compound [23]. Furthermore, the curvedness (Figure S4b) confirms this with the large flat areas of the surface which is outlined in blue.To check the mechanical stability of the crystal, a void analysis was performed to inspect the “empty” regions of the crystal structure,based on the

 doi:10.20944/preprints202410.0601.v1

isosurfaceof theprocrystal electron densities of the spherically symmetric atoms contained in the asymmetric unit [27]. Figure 5 is the graphical representation of voids in the crystal packing of 3,4-DAPP. The volume of the voids is 14.27 $Å^3$ and the percentage of free space in the unit cell is3.5%, which indicates the absence of any large cavity in the crystal,and the molecules are packed tightly, thereby this compound is expected to have a good mechanical properties [28,29].

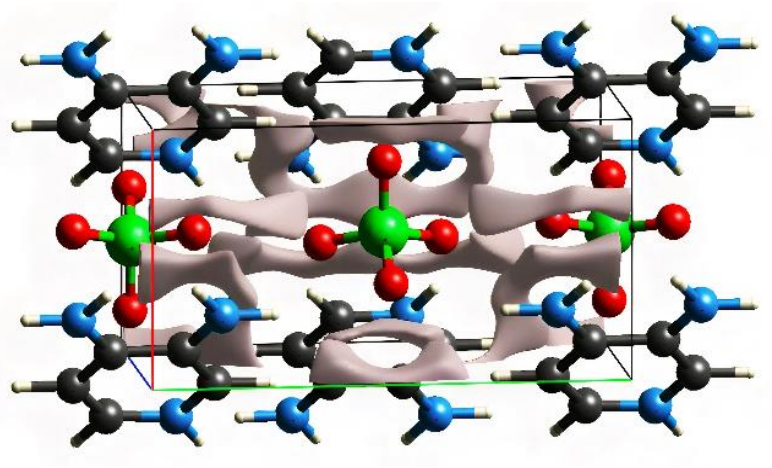

Figure 5. 3D graphical view of voids in the crystal packing of $(C_5H_8N_3)ClO_4$.

3.4. Thermal Analysis:

The thermal stability of the reported compound was studied using thermogravimetric analysis (TGA-DTG) and differential scanning calorimetry (DSC).The TGA-DTG curve results (Figure 6) showed that the investigated compound had thermal stability up to 285 °C with three weight loss stages. The first weight loss peak of 5.5% observed in the DTG curve at 285 °C may indicate the beginning of crystal decomposition. The second weight loss of 17.1% occurs in the temperature range of approximately 300–400 °C due to the decomposition of the organic moieties. The DTG curve shows a large weight loss of 31.8% at 387 °C, which is likely due to the decomposition of the remaining organic framework and possibly perchlorate decomposition. In addition, the DSC measurement was recordedin order to determine the exact phase transition temperatures. The diagram (Figure S4) showsone exothermic peak that appears at T = 50°C,attributed to the loss of surface water molecules, and the significant peak at T= 270 °C is attributed to the melting of the compound.

 doi:10.20944/preprints202410.0601.v1

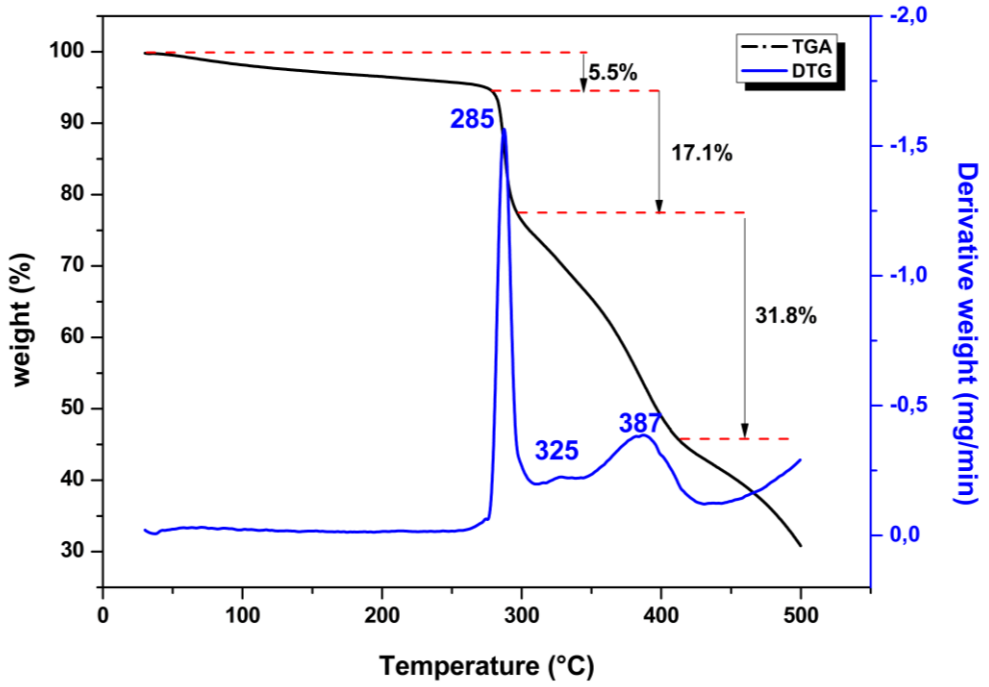

Figure 6. TGA/DTG thermogram of 3,4-DAPP.

3.5. Optical Study:

Todetermine the optical band gapof 3,4-DAPP, UV-vis diffuse reflectance was carried out. Figure 7 shows the variation of the reflectance (%) of the studied compound according to a function of the incident wavelength λ. The reflectance spectrum revealsthat the material exhibits strong absorption in the UV region, particularly below 400 nm, highlighting significant electronic transitions. Beyond 600 nm, the reflectance increases and stabilizes, suggesting higher reflectivity in the visible and near-infrared regions. The first derivative of the reflectance curve highlights a critical transition at 3.58 eV, corresponding to the material's band gap. Similarly, the absorbance spectrum (Figure S6) shows strong absorption in the UV absorption, particularly at wavelengths below 300 nm; further indicating key electronic transitions related to the band gap. As the wavelength increases, the absorbance gradually decreases, suggesting that the material becomes more transparent in the visible and near-infrared regions. The first derivative of the absorbance depicted in the inset Figure S6, indicates a significant transition estimated at 3.6 eV, which corresponds to the material's band gap and aligns with the typical range of large band gaps found in semiconductor materials [30,31]. This wide value is consistent with its high absorbance in the UV range and lower absorbance in the visible spectrum. Generally, the most important criterion for designing an efficient optoelectronic device is a wide band gap to ensure transparency to light in a particular wavelength range.

 doi:10.20944/preprints202410.0601.v1

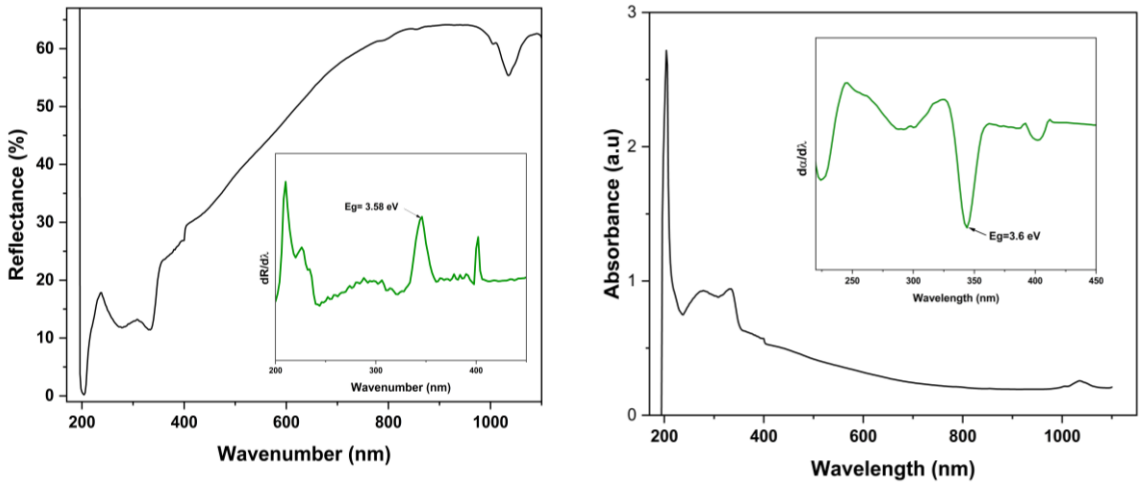

Figure 7. Evolution of the reflectanceand absorbance of 3,4-DAPP according to the wavelength λ. The insets illustrate the first derivative of each specter versus λ.

The CIE chromaticity coordinates (x=0.4426, y=0.3718) indicate that it emits green-yellow light close to the white point on the CIE diagramshown in Figure 8, suggesting a balanced emission across the visible spectrum. This position is near the white pointindicating lower color purity, meaning the emitted color is likely a mix of wavelengths and the color is relatively desaturated, resembling a soft, light pastel shade rather than a fully vibrant hue.These analyses suggest that the materialis characterized by strong UV absorption and high reflectance in the visible spectrummaking it potentially suitable forapplications in optoelectronics, UV-sensitive devices, or coatings, that require strong UV absorption and high visible reflectivity.

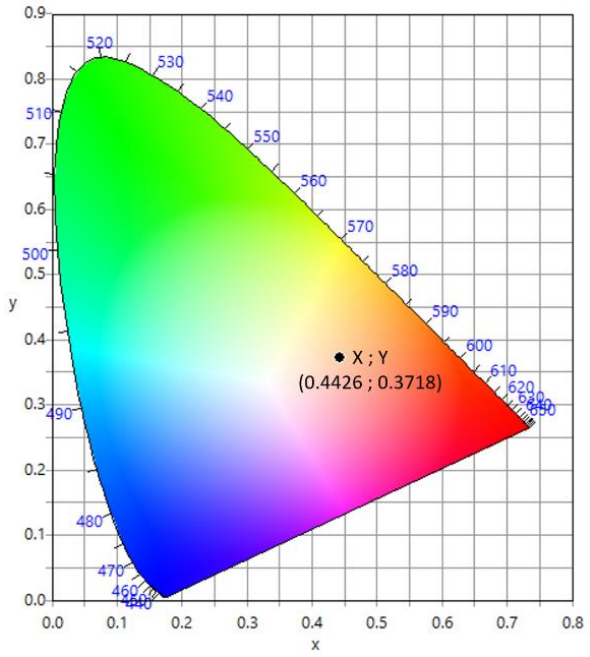

Figure 8. CIE chromaticity coordinate for3,4-DAPP.

3.6. DFT Analysis:

In order to reach more accurate assignments of the observed features in the context of molecular orbital, we optimized a deeper analysis for the geometry of 3,4-DAPP with the density functional theory (DFT) using a 6–31G+ basis set.The electron transition from the highest occupied molecular orbital (HOMO) to the lowest unoccupied molecular orbital (LUMO) creates a gap energy, and this

 doi:10.20944/preprints202410.0601.v1

latter is a critical parameter that determines the kinetic stability, chemical reactivity, optical polarizability, and chemical hardness-softness of the molecule [32].According to the analysis of the orbital contribution, the HOMO orbital is localizedmainly on the organic molecule (3,4-DAP) and partly on the perchlorate anions, while the LUMO orbital is located on the cationic part.The energies of HOMO and LUMO are -6.6957 and -2.3922eV, respectively, and the energy gap between these two orbitals is 4.3 eV (Figure 9), which is worth noting that the DFT results are appropriate as compared to the experimental value obtained by photoluminescence andsuggesting that the title compound indicate high chemical hardness and kinetically stable [33].As a matter of fact, this outcome indicates that this compound is a good candidate for a semiconducting device.

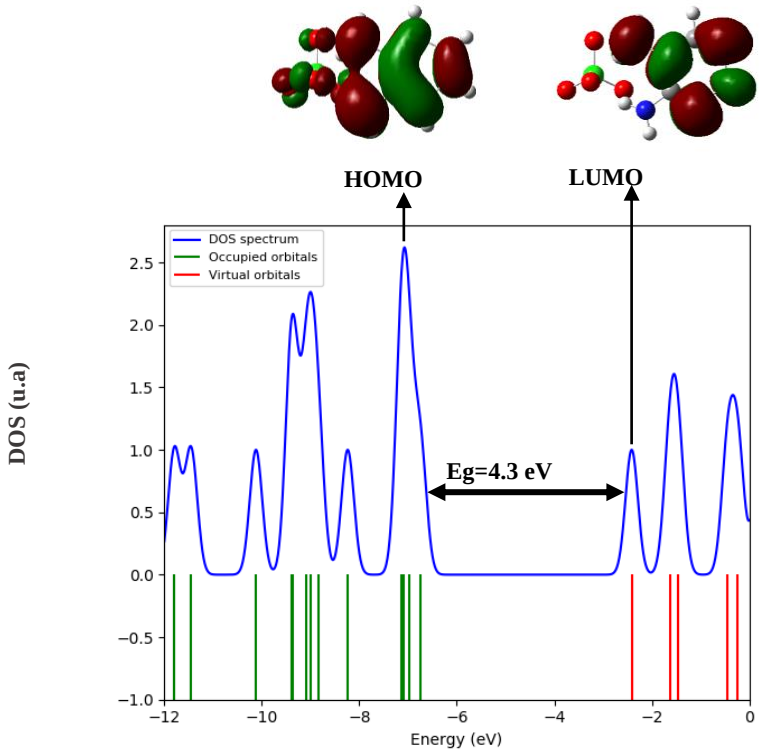

Figure 9. DOS plot and calculated HOMO-LUMO orbitals of 3,4-DAPP.

3.7. In-Vitro Antibacterial Results

The antimicrobial activity of the compound 3,4 DAPP was evaluated against gram-positive (*Staphylococcus aureus*, *Bacillus cereus,* and *Bacillus subtilis*) and gram-negative bacteria (*Pseudomonas aeruginosa*, *Enterococcus faecalis* and *Salmonella typhimurium*) by the agar well diffusion method (as shown in Figure 10). The 3,4-diaminopyridine (3,4-DAP) and gentamicin antibiotic were used as controls. The inhibition zone depends on the tested compound and the tested bacteria. Indeed, we demonstrated that 3,4-DAPP (50 mg/ml) showed an inhibition zone of about 10 mm slightly higher than 3,4-DAP (7 mm) towards *Bacillus cereus*. This activity disappears when we increase the concentration to (100 mg/ml) of both 3,4-DAPP and the 3,4-DAP. In addition, we demonstrated that 3,4-diaminopyridine (50 mg/ml) showed an inhibition zone of about 10 mm and 9 mm for both *Staphylococcus aureus* and *Bacillus subtilis*, respectively. These inhibition zones increased when we used the concentration of 100 mg/ml. These results prove the effectiveness of 3,4-DAP against these 2 bacteria. Unfortunately, the addition of the perchlorate group in 3,4-DAPP reduced this activity since we didn't find any inhibition zone of 3,4 DAP against *Staphylococcus aureus* and *Bacillus subtilis* (Table 2, Figure 10). On the other hand, the 3,4-diaminopyridine (50 mg/ml) was active against *Enterococcus faecalis* (14 mm) and *Pseudomonas aeruginosa* (14 mm), this activity decreases to 8 mm and disappears with the 3,4-DAPP compound (50 mg/ml) towards these two bacteria, respectively.This result further confirms that the addition of the acid group in the newly synthesized molecule was

 doi:10.20944/preprints202410.0601.v1

ineffective against *Enterococcus faecalis* and *Pseudomonas aeruginosa*[34]. Moreover, both 3,4 DAPP and 3,4-diaminopyridine are inactive against *Salmonella thyphi*. The gentamicin used as positive control showed an important inhibition zone of about 32-40 mm (Table 2, Figure 10). Looking forward, our perspectives include expanding our analysis to test our compound against Alzheimer's disease, exploring its potential as a therapeutic agent for neurodegenerative conditions, and further understanding its mechanism of action in different biological contexts.

Table 2. Inhibition Zone (mm) of 3,4-DAPP and CO against bacteria.

Bacteria	*Inhibition zone (mm)*					
	3,4 DAPP		CO		ATB	C-
	50	100	50	100		
Staphylococcus aureus	**-**	**-**	**10**	**17**	**34**	**0**
Bacillus subtilis	**-**	**-**	**9**	**15**	**40**	**0**
Bacillus cereus	**10**	**0**	**7**	**0**	**35**	**0**
Enterococcus faecalis	**8**	**-**	**14**	**15**	**33**	**0**
Pseudomonas aeruginosa	**-**	**-**	**14**	**16**	**43**	**0**
Salmonella typhimurium	**-**	**-**	**-**	**-**	**32**	**0**

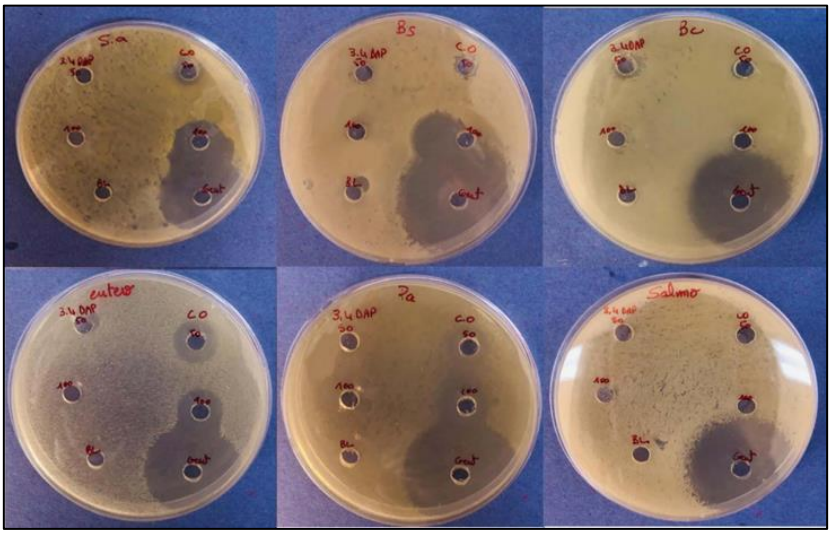

Figure 10. Inhibition zone (mm), of 3,4-DAPP, CO (3,4-DAP) and ATB (antibiotic) against bacteria: **Sa:** Staphylococcus aureus, **Bs:**Bacillussubtilis, **Bc:** Bacillus cereus, **Entero:**Enterococcus faecalis, **Pa:** Pseudomonas aeruginosa, **Salmo:** Salmonella typhimurium**.**

4. Conclusions

In this reported research, we prepared and characterized a new non-centrosymmetric hybrid compound based on aminopyridine derivate (3,4-diaminopyridin) and perchlorate salt. The crystallographic data show that this compound crystallizes in the monoclinic system with the space group $P2_1$ and the supramolecular structure isstabilized by weak hydrogen interactions (H···O).In addition, the volume fraction occupied by cavities voids indicates the mechanical strength of the structure. Thermal studies (TGA) and DSC were used to confirm the composite phase transition and the high thermal stability, while the opticalproperties indicate the green-yellow luminescence characteristic.Furthermore, the molecular orbitals studied by DFT theory confirm the semiconducting properties of the studied compound. Additionally, Biological activity tests revealed that 3,4-DAPP exhibited moderate antibacterial activity, particularly against Bacillus cereus, but was less effective than 3,4-DAP against other bacteria, suggesting the perchlorate group may reduce its antimicrobial efficacy.

 doi:10.20944/preprints202410.0601.v1

Supplementary Materials: The following supporting information can be downloaded at the website of this paper posted on Preprints.org.

Accession Codes: CCDC 2300737contains the supplementary crystallographic data for this paper. These data can be obtained free of charge via www.ccdc.cam.ac.uk/data_request/cif, or by emailing data_request@ccdc.cam.ac.uk, or by contacting The Cambridge Crystallographic Data Centre, 12 Union Road, Cambridge CB2 1EZ, UK; fax: +44 1223 336033.

References

1. S. Sathiyakumar, P. Selvam, S. Antharjanam, F.L. Hakkim, K. Srinivasan, W.T.A. Harrison; Mechano-chemical syntheses of new cobalt (II) complexes ofalkyl 2- (pyridine-eyl-methylene) hydrazinecarboxylates: crystal structures, spectroscopic and photoluminescence properties;J. Mol. Struct. 1205 (**2020**) 127666, https://doi.org/10.1016/j.molstruc.2019.127666.
2. S.A. Zarei; A mononuclear cobalt(II) salophen-type complex: Synthesis, theoretical and experimental electronic absorption and infrared spectra, crystal structure, and predicting of second- and third-order nonlinear optical properties; J. Spectrochim, Acta A 215 (**2019**) 225, https://doi.org/10.1016/j.saa.2019.02.083
3. K. Kahouli, A.B. Kharrat, S. Chaabouni; Optical properties analysis of the new $(C_9H_{14}N)_3BiCl_6$ compound by UV–visible measurements; Indian J. Phys. 95 (**2021**) 2797, https://doi.org/10.1007/s12648-020-01942-w
4. D. Pandiarajan, R. Rengan;Ruthenium (II) half-sandwich complexes containing thioamides: Synthesis, structures and catalytic transfer hydrogenation of ketones;J. Org. Chem 723 (**2013**) 26, https://doi.org/10.1016/j.jorganchem.2012.10.003
5. W. Mao, J. Wang, X. Hu, B.Zhou, G. Zheng, S. Mo, S. Li, F. Long, Z. Zou; Synthesis, crystal structure, photoluminescence properties of organic-inorganic hybrid materials based on ethylenediamine bromide; J. Saudi Chemical Society 24 (**2019**) 52, https://doi.org/10.1016/j.jscs.2019.09.003
6. A. Vakulka, E. Goreshnik, M. Jagodic, Z. Jaglicic, Z. Trontelj;Tetrahydrated bis(ethylenediamine)copper(II) sulfate: Crystal structure, Raman spectrum and magnetic susceptibility;J. Mol. Struct. 1210 (**2020**) 128002, https://doi.org/10.1016/j.molstruc.2020.128002
7. J. Molgo, M. Lemeignan, F. Peradejordi;P.Lechat ;Presynaptic effects of aminopyridines on the neuromuscular junction of vertebrates ; J Pharmacology 16 (**1985**) 10, PMID: 2417060.
8. G.E. Kirsch, T. Narahashi; 3,4-diaminopyridine. A potent new potassium channel blocker; J Biophys 22 (**1978**) 507, DOI: 10.1016/S0006-3495(78)85503-9
9. S.R. Schwid, M.D. Petrie, M.P. McDermott, D.S. Tierney, D.H. Maso, A.D. Goodman;Quantitative assessment of sustained-release 4-aminopyridine for symptomatic treatment of multiple sclerosis; J. Neurology 48 (**1997**) 817, https://doi.org/10.1177/135245859600200517
10. K.M. McEvoy, A.J. Windebank, J.R. Daube, P.A. Low; 3,4-Diaminopyridine in the Treatment of Lambert–Eaton Myasthenic Syndrome; J. Med 321 (**1989**) 1567, DOI: 10.1056/NEJM198912073212303
11. M. Messaad, I. Dhouib, M. Abdelhedi, B. Khemakhem; Synthesis, bioassay and molecular docking of novel pyrazole and pyrazolone derivatives as acetylcholinesterase inhibitors; J. Mol. Struct. 1263 (**2022**) 133105, https://doi.org/10.1016/j.molstruc.2022.133105
12. C. Carlsson, I. Rosen, E. Nilsson; Can 4-Aminopyridine be Used to Reverse Anaesthesia and Muscle Relaxation; J. Acta AnaesthesiolScand 27 (**1993**) 87, https://doi.org/10.1111/j.1399-6576.1983.tb01911.x
13. I. Bayar, L. Khedhiri, R. Fezai, P.S.P. da Silva, M.R. Silva, C. Nasr; A hybrid perchlorate with a low band gap: Crystal structure, physicochemical characterization and Hirschfeld surfaces study; J. Mol. Struct. 1181 (**2019**) 300, https://doi.org/10.1016/j.molstruc.2018.12.096
14. J. Janczak, G.J. Perpétuo; Supramolecular aggregation in new crystals with nonlinear optical properties: 2-aminophenol-$HClO_4$, 3-aminophenol-$HClO_4$ and 4-aminophenol-$HClO_4$; J. Solid State Sciences 11 (**2009**) 1576, https://doi.org/10.1016/j.solidstatesciences.2009.06.024
15. B.B. Koleva, T. Kolev, T. Tsanev, S. Kotov, H. Mayer-Figge, Rûdiger, W. Seidel, W.S. Sheldrick; Crystal structure, optical and magnetic properties of the bis(perchlorate) of 3,4-diaminopyridine; J. Struct. Chem. 19 (**2008**) 13, DOI 10.1007/s11224-007-9236-0
16. M.A. Spackman, P.G. Byrom ; A novel definition of a molecule in a crystal ; Chem. Phys. Lett. 267 (**1997**) 215, https://doi.org/10.1016/S0009-2614(97)00100-0
17. L.J. Farrugia;WinGX suite for small-molecule single-crystal crystallography; J. Appl. Crystallogr. 32 (**1999**) 837, https://doi.org/10.1107/S0021889899006020
18. G.M. Sheldrick, Crystal structure refinement with SHELXL; J. Acta Cryst. 71 (**2015**) 3, doi:10.1107/s2053229614024218
19. M.A. Spackman, D. Jayatilaka;Hirshfeld surface analysisJ.Cryst. Eng. Comm. 11 (**2009**) 19, DOI: 10.1039/B818330A
20. M.J. Frisch, G.W. Trucks, H.B. Schlegel, G.E. Scuseria, M.A. Robb, J.R. Cheeseman, G. Scalmani, V. Barone, B. Mennucci, G.A. Petersson, H. Nakatsuji, M. Caricato, X. Li, H.P. Hratchian, A.F. Izmaylov, J. Bloino, G. Zheng, J.L. Sonnenberg, M. Hada, M. Ehara, K. Toyota, R. Fukuda, J. Hasegawa, M. Ishida, T. Nakajima, Y.

Honda, O. Kitao, H. Nakai, T. Vreven, J.A. Montgomery, Jr., J.E. Peralta, F. Ogliaro, 1 M. Bearpark, J.J. Heyd, E. Brothers, K.N. Kudin, V.N. Staroverov, R. Kobayashi, J. Normand, K. Raghavachari, A. Rendell, J.C. Burant, S.S. Iyengar, J. Tomasi, M. Cossi, N. Rega, J.M. Millam, M. Klene, J.E. Knox, J.B. Cross, V. Bakken, C. Adamo, J. Jaramillo, R. Gomperts, R.E. Stratmann, O. Yazyev, A.J. Austin, R. Cammi, C. Pomelli, J.W. Ochterski, R.L. Martin, K. Morokuma, V.G. Zakrzewski, G.A. Voth, P. Salvador, J.J. Dannenberg, S. Dapprich, A.D. Daniels, Ö. Farkas, J.B. Foresman, J.V. Ortiz, J. Cioslowski,, D.J. Fox, Gaussian 09, Gaussian, Inc., Wallingford CT (**2009**).

21. A.R. Allouche, Gabedit is a free Graphical User Interface for computational chemistry packages; J. Computational Chem. 32 (**2010**) 174, **https://doi.org/10.1002/jcc.21600**
22. L. Mary Novena, S. Suresh Kumar, S. Athimoolam; Improved solubility and bioactivity of theophylline (a bronchodilator drug) through its new nitrate salt analysed by experimental and theoretical approaches; J. Mol. Struct. 1116(**2016**) 45, https://doi.org/10.1016/j.molstruc.2016.03.01
23. N. Elleuch, D. Fredj, N. Chniba-Boudjada, M. Boujelbene; Synthesis of a New Chloro Antimony Complex with Pyridinium Derivative: Crystal Structure, Hirshfeld Surface Analysis, Vibrational, and Optical Properties; J. Inorg. and Organometallic Polymers and Materials 30 (**2019**) 889, https://doi.org/10.1007/s10904-019-01316-8
24. J. Bernstein, R. E. Davis, L. Shimoni et N. -L. Chang; Patterns in Hydrogen Bonding: Functionality and Graph Set Analysis in Crystals; J. AngewandteChemie International Edition, 34 (**1995**) 1555, **https://doi.org/10.1002/anie.199515551**
25. J. Zaleski and A. Pietraszko; Structure at 200 and 298 K and X-ray investigations of the phase transition at 242 K of $[NH_2(CH_3)_2]_3Sb_2Cl_9$ (DMACA); J. Acta Crystallogr. B 52 (**1996**) 287, **https://doi.org/10.1107/S0108768195010615**
26. Y.H. Luo, G.G. Wu, S. L Mao, B.W. Sun; Complexation of different metals with a novel N-donor bridging receptor and Hirshfeld surfaces analysis; J. InorgChim Acta 397 (**2013**) 1, https://doi.org/10.1016/j.ica.2012.11.010
27. M. J. Turner,J. J. McKinnon, , D. Jayatilaka,, Spackman ; M. A. ; Visualisation and characterisation of voids in crystalline materials;J. CrystEngComm, 13 (**2011**) 1804, https://doi.org/10.1039/C0CE00683A
28. E. Irrou, Y.A. Elmachkouri, A. Oubelle, H. Ouchtak, S. Dalbouha, J.T. Mague, T. Hökelek, L. El Ghayari, N.K. Sabber, and M.L. Taha; Crystal structure determination, Hirshfeld surface, crystal void, intermolecular interaction energy analyses, as well as DFT and energy framework calculations of 2-(4-oxo-4,5-dihydro-1H-pyrazolo- [3,4-d] pyrimidin-1-yl)acetic acid; J. Acta Cryst. E 78 (**2022**) 953, https://doi.org/10.1107/S2056989022008489
29. M. Kurbanova, M. Ashfaq, M. N. Tahir, A. Maharramov, N. Dege, N. Ramazanzade, E. B. Cinar; synthesis, crystal structure, supramolecular assembly inspection by hirshfeld surface analysis and computational exploration of 4-phenyl-6-(*p*-TOLYL) pyrimidin-2 (1H)-one (PPTP); J. Struct. Chem. 64 (**2023**) 437, DOI: 10.1134/S0022476623030095
30. B.B. Ivanova, M.G. Arnaudov, H. Mayer-Figge; Molecular spectral analysis and crystal structure of the 4-aminopyridinium tetrachloropalladate (II) complex salt; J. Polyhedron 24 (**2005**) 1624, https://doi.org/10.1016/j.poly.2005.04.028
31. I. Bayar, L. Khedhiri, F. Lefebvre, V. Ferretti, C.B. Nasr; Crystal structure, Hirshfeld surfaces computational study and physicochemical characterization of two new organic salts of 2-chlorobenzylamine, $(ClC_7H_6NH_3)\cdot NO_3$ and $(ClC_7H_6NH_3)\cdot ClO_4$; J. Mol. Struct. 1179 (**2018**) 171, https://doi.org/10.1016/j.molstruc.2018.10.081
32. K. Efil, Y. Bekdemir; Theoretical and experimental investigations on molecular structure, IR, NMR spectra and HOMO-LUMO analysis of4-methoxy-N-(3-phenylallylidene) aniline;Am. J. of Phy. Chem. 3 (**2014**), 19, doi: 10.11648/j.ajpc.20140302.13
33. I. Bayar, L. Khedhiri, E. Jeanneau, F. Lefebvre, C.Ben Nasr; Synthesis, structural study and characterization of two new $(ClC_7H_6NH_3)ClO_4.H_2O$ isostructural hydrates of isomeric organic amine perchlorates; J. Mol. Struct. 1211 (**2020**) 128078, https://doi.org/10.1016/j.molstruc.2020.128078
34. L. Mary Novena, S. Suresh Kumar, S. Athimoolam; Improved solubility and bioactivity of theophylline (a bronchodilator drug) through its new nitrate salt analysed by experimental and theoretical approaches; J. Mol. Struct. 1116 (**2016**) 45, https://doi.org/10.1016/j.molstruc.2016.03.014